sciendo

Int. J. of Applied Mechanics and Engineering, 2020, vol.25, No.4, pp.69-83
DOI: 10.2478/ijame-2020-0050

MATHEMATICAL MODELING OF CONVECTIVE HEAT AND MASS TRANSFER OF A ROTATING NANO-FLUID BOUNDED BY STRETCHING AND STATIONARY WALLS IN A VERTICAL CONDUIT

B. HARITHA
Department of Mathematics, Santhiram Engineering College
Nandyal, Andra Pradesh, INDIA

C. UMADEVI
Department of Mathematics, TKRCET, Hyderabad
Telangana, INDIA

M.Y. DHANGE*
Department of Mathematics, B.L.D.E.A's V.P. Dr. P.G. Halakatti College
of Engineering and Technology
Vijayapur, Karnataka, INDIA
E-mail: math.mallinath@bldeacet.ac.in

The influence of thermal emission and unvarying magnetic field of convective heat and mass transfer of a rotating nano-liquid in an upright conduit constrained by a stretching and motionless wall is studied. The temperature, concentration profile, primary and secondary velocities have been computed through similarity transformation and fourth-order Runge-Kutta shooting technique. The objective of this article is to measure the impact of emission constraint, Brownian movement constraint and Eckert number, thermophoresis constraint, Prandtl number, space, and temperature-dependent heat source constraint on velocity. The results are presented in tables and graphs. Further, various constraint impacts on the skin friction coefficient, heat and mass transfer rates are also explored. This work is pertinent to biotechnological and engineering uses, like mass and heat transfer enhancement of microfluids and design of bioconjugates.

Key words: Brownian motion, magnetic field, stretching wall, vertical conduit, thermophoresis.

1. Introduction

The word "*nanofluid*" referres to a liquid suspension having ultra-fine particles (diameter < *50 nm*) (Choi [1]). Conventional fluids (for example, water, mineral oils, ethylene glycol, motor oil, and so on) utilized for heat transfer applications have limited heat transfer abilities. Nanofluids are the engineered colloidal suspension of nanometer-sized particles of metals and metallic oxides such as copper, aluminum, iron, gold, and titanium or their oxides in base fluids. Water, ethylene glycol, oil, bio-liquids, and toluene are typical base fluids. Experimental research revealed that base liquids with the suspension of nanoparticles have significantly higher thermal conductivities than those of the base fluids. Investigation of convective heat transfer in nanofluids has become a subject of contemporaneous enthusiasm because of its applications in a few ventures, for example, power plant activities, manufacturing and transportation, electronics cooling, heat exchangers, and delivery of nano-drug. Limited studies have been reported in literature [2]-[5].

The fluid flow due to a stretching surface has key applications e.g. in the manufacture of glass and paper sheets, hot rolling, metallic spiraling, the depiction of plastic films, and extrusion of metals and

* To whom correspondence should be addressed

polymers. Bachok *el al*. [6] numerically investigated the steady boundary layer movement of a nanofluid over a moving semi-infinite plate in a uniform free stream. Some researchers [7]-[17] have studied the boundary layer movement and stretching surface of a nanofluid with heat and mass transfer analysis under various circumstances.

The magneto-hydrodynamics has significant applications in material processing and engineering, e.g. in MHD-generators, devices in industry, nuclear-powered reactors. The MHD-liquid flow in a rotating conduit is an exciting area. Hazem [18] studied the MHD-flow of an electrically conducting, viscous, and incompressible liquid in an infinite rotating porous disk. The liquid was subject to an external uniform magnetic field perpendicular to the plane of the disk. After this study, a few investigators have studied the MHD impacts on the boundary layer movement and stretching surface of a nanofluid with convective heat and mass transfer flow in various circumstances [19]-[25].

The present article investigates the effects of emission constraint, chemical response constraint, Eckert number, Brownian movement constraint, magnetic field, thermophoresis constraint, space/temperature-dependent heat source constraints, Prandtl number and Lewis number, on the velocity, temperature, and concentration profile. The results are discussed numerically through graphs and tables.

2. Mathematical formulation and methodology

Consider a steady 2-dimensional laminar convective heat and mass transfer stream of a viscous electrically conducting liquid in an upright conduit constrained by a stretching sheet on the left and a fixed plate on the right. Figure 1 presents a schematic graph of the problem. The unvarying magnetic field of strength H_o is applied normal to the dividers of the conduit. We assume magnetic Reynolds number (R_m) to be small and ignore the induced magnetic field in comparison to the applied magnetic field. It is additionally assumed that there is no applied polarization and body couple, consequently no electric field.

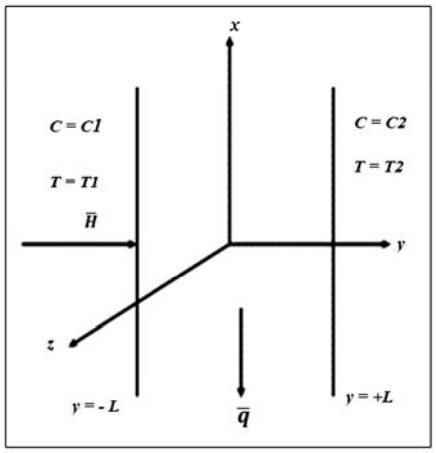

Fig.1. Schematic graph.

The nano-particle concentration, velocity, and temperature are specified in the subsequent form

$$\overline{q} = (u(x,y), v(x,y), w(x,y)), \quad T = T(x,y), \quad C = C(x,y). \tag{2.1}$$

Taking the viscous dissipation and Joule warming impacts into consideration, the important flow conditions of the problem are expressed as

$$\frac{\partial u}{\partial x} + \frac{\partial v}{\partial y} = 0, \tag{2.2}$$

$$u\frac{\partial u}{\partial x}+v\frac{\partial u}{\partial y}=-\frac{1}{\rho_f}\frac{\partial p}{\partial x}+\nu\left(\frac{\partial^2 u}{\partial x^2}+\frac{\partial^2 u}{\partial y^2}\right)+\left(\frac{2\Omega}{\rho_f}\right)w-\left(\sigma\mu_e^2H_o^2/\rho_f\right)u+$$
$$\frac{1}{\rho_f}\left[(1-C_o)\rho_f\beta g(T-T_2)\right]-\frac{(\rho_p-\rho_f)g(C-C_o)}{\rho_f}, \tag{2.3}$$

$$u\frac{\partial v}{\partial x}+v\frac{\partial v}{\partial y}=-\frac{1}{\rho_f}\frac{\partial p}{\partial y}+\nu\left(\frac{\partial^2 v}{\partial x^2}+\frac{\partial^2 v}{\partial y^2}\right), \tag{2.4}$$

$$u\frac{\partial w}{\partial x}+v\frac{\partial w}{\partial y}=\nu\left(\frac{\partial^2 w}{\partial x^2}+\frac{\partial^2 w}{\partial y^2}\right)-\left(\sigma\mu_e^2H_o^2/\rho_f\right)w-\left(\frac{2\Omega}{\rho_f}\right)u, \tag{2.5}$$

$$u\frac{\partial T}{\partial x}+v\frac{\partial T}{\partial y}=\frac{k_f}{\rho_f C_p}\left(\frac{\partial^2 T}{\partial x^2}+\frac{\partial^2 T}{\partial y^2}\right)+\tau\left\{D_B\frac{\partial T}{\partial y}\frac{\partial C}{\partial y}+\frac{D_T}{T_\infty}\left(\frac{\partial T}{\partial y}\right)^2\right\}+q'''+$$
$$-\frac{\partial(q_R)}{\partial y}+\frac{2\mu}{\rho_f C_p}\left(\left(\frac{\partial u}{\partial y}\right)^2\left(\frac{\partial w}{\partial y}\right)^2\right)+\left(\frac{\sigma\mu_e^2H_o^2}{\rho_f C_p}\right)\left(u^2+w^2\right), \tag{2.6}$$

$$u\frac{\partial C}{\partial x}+v\frac{\partial C}{\partial y}=D_B\left(\frac{\partial^2 C}{\partial x^2}+\frac{\partial^2 C}{\partial y^2}\right)-kc(C-C_0)+\frac{D_T k_T}{T_m}\left(\frac{\partial^2 T}{\partial x^2}+\frac{\partial^2 T}{\partial y^2}\right), \tag{2.7}$$

$$\rho-\rho_o=-\beta(T-T_o)-\beta^*(C-C_o) \tag{2.8}$$

where, μ_e, k, g, D_T, p, K_T, μ, σ, ρ, β, β^*, T, u, D_B, C, v, $\tau=\dfrac{(\rho C_p)_p}{(\rho C_p)_f}$ are the magnetic permeability of the medium, permeability of the porous medium, gravity, thermophoresis dispersal coefficient, pressure, thermal dispersal ratio, dynamic viscosity, average liquid temperature, electrical conductivity, density of liquid, thermal growth coefficient, volume growth coefficient, dimensional temperature, *x*- direction velocity component, Brownian dispersion coefficient, concentration of nanoparticle, *y*- direction velocity component and nanoparticle heat and base fluid heat capacity ratio, respectively.

The inner heat generation/absorption q''' is shown as

$$q'''=\frac{k_f us}{x\nu}\left(A_1\left(T_1-T_2\right)u+B_1\left(T-T_2\right)\right) \tag{2.9}$$

where A_1 is the space dependent coefficient and B_1 is the temperature dependent coefficient. It is noticed that $A_1>0$ and $B_1>0$ and $A_1<0$ and $B_1<0$ correspond to the inner heat generation and inner heat absorption, respectively.

Applying the Rosseland approximation, we get

$$q_r=-\frac{4\sigma^\bullet}{3\beta_R}\frac{\partial T'^4}{\partial y},\qquad T'^4\cong 4TT_o^3-3T_0^4,\qquad \frac{\partial q_R}{\partial z}=-\frac{16\sigma^\bullet T_0^3}{3\beta_R}\frac{\partial^2 T}{\partial y^2}. \tag{2.10}$$

where $\sigma^{\bullet}$ is the Stefan-Boltzman constant and β_R is the average absorption coefficient.

Nano-particle concentration, velocity, and temperature boundary conditions are specified as follows

$$u(x,-L)=bx,\quad u(x,+L)=0,\quad v(x,\pm L)=0,\quad T(x,-L)=T_1,$$
$$T(x,+L)=T_2 C(x,-L)=C_1,\quad C(x,+L)=C_2 \tag{2.11}$$

where $b>0$, T_1, T_2 ($T_1>T_2$), C_1, C_2 ($C_1>C_2$) are the rate of stretching conduit wall, static temperatures and concentrations of the left and right dividers, respectively.

The associated similarity variables are

$$\eta=\frac{y}{L};\quad u=bxf'(\eta);\quad v=-bLf(\eta);\quad w=bxg(\eta);\quad \theta(\eta)=\frac{T-T_2}{T_1-T_2};\quad \phi(\eta)=\frac{C-C_2}{C_1-C_2}. \tag{2.12}$$

Removing the pressure in Eqs (2.3) and (2.4) and using Eq.(2.10), the momentum condition is

$$f^{iv}+\mathrm{Re}\,x(f'''f'-ff'')-M^2f''+\mathrm{Gr}(\theta'-N\varphi')+Rg'=0. \tag{2.13}$$

$$g''+\mathrm{Re}\,x(fg'-f'g)-M^2g-Rf'=0, \tag{2.14}$$

while Eqs (2.6) and (2.7) taking into account Eqs (2.9), (2.10), and (2.12) are

$$\left(1+\frac{4Nr}{3}\right)\theta''+\mathrm{Pr}\,\mathrm{Re}\,x(f\theta')+A_{11}f'+B_{11}\theta+\mathrm{Pr}\,\mathrm{Ec}\left(\left(f''\right)^2+\left(g'\right)^2\right)+$$
$$+M^2\mathrm{Ec}\left((f')^2+g^2\right)+\mathrm{Pr}\,Nb(\theta'\varphi')+\mathrm{Pr}\,Nt(\theta')^2, \tag{2.15}$$

$$\varphi''+\mathrm{Le}\,\mathrm{Re}\,x\left(f\varphi'\right)-\mathrm{Le}\gamma(\varphi)+\left(\frac{Nt}{Nb}\right)\theta''=0 \tag{2.16}$$

where, $\mathrm{Gr}=\frac{\beta g(T_1-T_2)L}{bx}$ is the Grashof number, $M^2=\frac{\sigma\mu_e^2H_o^2L^2}{\nu x}$ is the magnetic constraint, $N=\frac{(\rho_p-\rho_f)(C_1-C_2)}{(1-C_o)\rho_f\beta(T_1-T_2)}$ is the buoyancy ratio constraint, $\mathrm{Pr}=\frac{\mu C_p}{k_f}$ is the Prandtl number, $A_{11}=\frac{A_1b^2x}{\nu}$ is the space dependent heat source constraint, $B_{11}=\frac{B_1b}{\nu}$ is the temperature dependent heat source constraint, $\mathrm{Re}\,x=\frac{bL^2}{\mu}$ is the local Reynolds number, $\mathrm{Le}=\frac{\nu}{D_B}$ is the Lewis number, $\gamma=\frac{kcL^2}{D_B}$ is the chemical response constraint, $\mathrm{Ec}=\frac{b^2x^2}{C_p\Delta T}$ is the Eckert number, $Nr=\frac{4\sigma^{\bullet}T_o^3}{\beta_r k_f}$ is the emission constraint,

$Nt = \dfrac{\left(\rho C_p\right)_p D_T \left(T_1 - T_2\right)}{\left(\rho C_p\right)_f T_o \nu}$ is the thermophoresis constraint, $Nb = \dfrac{(\rho C_p)_p D_B (C_1 - C_2)}{(\rho C_p)_f \nu}$ is the Brownian motion constraint.

Boundary conditions of Eq. (2.11), in interpretation of Eq. (2.12) are reduced as follows

$$f(-1) = 0, \quad f(+1) = 0, \quad f'(-1) = 1, \quad f'(+1) = 0, \quad g(-1) = 0, \quad g(+1) = 0,$$
$$\theta(-1) = 1, \quad \theta(+1) = 0, \quad \phi(-1) = 1, \quad \phi(+1) = 0. \tag{2.17}$$

A standard methodology is to compose the nonlinear ODE in the form of a first order initial value problem as follows

$$f = f_1, \; f' = f_2 f'' = f_3, \; f''' = f_4, \; g = f_5, \; g' = f_6, \; \theta = f_7, \; \theta' = f_8, \; \phi = f_9, \; \phi' = f_{10}, \tag{2.18}$$

$$f^{iv} = f_4' = -\mathrm{Re}\, x\left[f_4 f_1 - f_2 f_3\right] + M^2 f_3 + \mathrm{Gr}\left(f_6 - N f_8\right) - R g', \tag{2.19}$$

$$g'' = f_6' = -\mathrm{Re}\, x\left[f_6 f_1 - f_2 f_5\right] + M^2 f_5 + R f_2, \tag{2.20}$$

$$\theta'' = f_8' = -[\mathrm{Pr}\,\mathrm{Re}\, x(f_1 f_8) + A_{11} f_2 + B_{11} f_7 - \mathrm{Pr}\,\mathrm{Ec}\left(f_3^2 + f_6^2\right) + -M^2 \mathrm{Ec}\left(f_2^2 + f_5^2\right) - \mathrm{Pr}\, Nb\left(f_8 f_{10}\right) - \mathrm{Pr}\, Nt\left(f_8^2\right)\Big] \Big/ \left(1 + \frac{4Nr}{3}\right), \tag{2.21}$$

$$\varphi'' = f_8' = [-\mathrm{Le}\,\mathrm{Re}\, x\left(f_1 f_{10}\right) + \mathrm{Le}\gamma f_9 - \left(\frac{N_t}{N_b}\right)\left(-\left[\mathrm{Pr}\,\mathrm{Re}\, x\left(f_1 f_8\right) + A_{11} f_2 + B_{11} f_7 + -\mathrm{Pr}\,\mathrm{Ec}\left(f_3^2 + f_6^2\right) - M^2 \mathrm{Ec}\left(f_2^2 + f_5^2\right) - \mathrm{Pr}\, Nb\left(f_8 f_{10}\right) - \mathrm{Pr}\, Nt\left(f_8^2\right)\right] \Big/ \left(1 + \frac{4Nr}{3}\right)\right). \tag{2.22}$$

The related boundary conditions are

$$f_1(-1) = 0, \quad f_1(+1) = 0, \quad f_2(-1) = 1, \quad f_2(+1) = 0, \quad f_5(-1) = 1, \quad f_5(+1) = 0,$$
$$f_6(-1) = 1, \quad f_6(+1) = 0, \quad f_7(-1) = 1, \quad f_7(+1) = 0, \quad f_8(-1) = 1, \quad f_8(+1) = 0. \tag{2.23}$$

A shooting method is applied here to solve the above system, which might be a blend of the Runge-Kutta technique and a 5-dimensional zero discovering algorithm. It is noted that the missing initial conditions are coupled with the goal that the solution satisfies the limit conditions $f(1)=0$, $f'(1)=0$, $g(1)=0$, $\theta(1)=0$, $\phi(+1)=0$ of the original boundary value problem; and $f_3(-1), f_4(-1), f_6(-1), f_8(-1), f_{10}(-1)$ are the unknown initial conditions.

3. Discussion

The non-linear governing equations have been solved by applying the fourth order Runge-Kutta-shooting method. The expressions for velocity (f' and g), temperature (θ) and concentration of nano-particles (φ) have been computed by using the *MATHEMATICA* and results are presented in graphs.

The effects of various constraints on primary and secondary velocities have been illustrated in Figs 2a, 2b, 3a, 3b, 4a, 4b, 5a, 5b, 6a, 6b, 7a, 7b, 8a, 8b, 9a, 9b, 10a, and 10b.

The primary and secondary velocity rises with an increase in the emission constraint (N_r), Eckert number (E_c), and Brownian movement constraint (N_b) monotonically (Figs 2a, 2b, 3a, 3b, 6a, 6b). The growth in the emission constraint, Eckert number and Brownian movement constraint increases the width of the boundary layer of the conduit walls, which enhances the velocities. In the case of an increase in the thermophoresis constraint (N_t), Lewis number (L_e), space dependent heat source constraint (A_{11}) and temperature dependent heat source constraint (B_{11}), the primary velocity rises (Figs 3a, 5a, 6a, 8a) but the secondary velocity decreases (Figs 3b, 5b, 6b, 8b). In the case of the Prandtl number (P_r), the primary velocity drops (Fig.9a) and the secondary velocity rises (Fig.9b) with an increase in the Prandtl number. Figures 10a and 10b clarify the influence of the magnetic constraint. It is observed that the existence of the magnetic constraint makes the velocity descend through the boundary layer. It confirms the fact that the Lorentz force acts as a retarding force. These outcomes are concurrent with the results of Khan-Pop [8] and Gorla-Chamkha [11].

It is noticed that temperature increases with increase in emission constraint, Eckert number, thermophoresis constraint, Brownian movement constraint, Lewis number, space dependent and temperature dependent heat source constraints (Figs 2c, 3c, 4c, 5c, 6c, 7c, and 8c) but it decreases with rise in the Prandtl number and magnetic constraint (Figs 9c, 10c). This is due to fact that the lesser the thermal diffusivity, the smaller the thermal boundary layer thickness and larger the salutal boundary layers. It is also observed that on increase in the emission constraint, Eckert number, Brownian movement constraint, thermophoresis constraint, and magnetic constraint, reduces the nano-particle concentration (Figs 2d, 3d, 4d, 7d, 10d) but it increases with the growth in the space dependent heat source constraint, temperature dependent heat source constraint, Lewis number and the Prandtl number (Figs 5d, 6d, 8d and 9d).

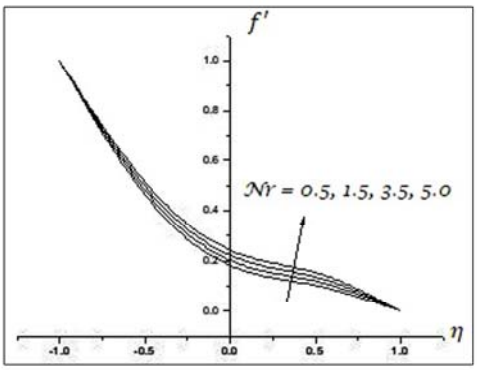

(a) Illustration of primary velocity (f') versus N_r.

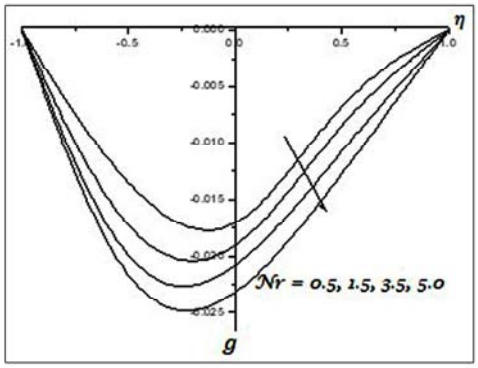

(b) Illustration of secondary velocity (g) versus N_r.

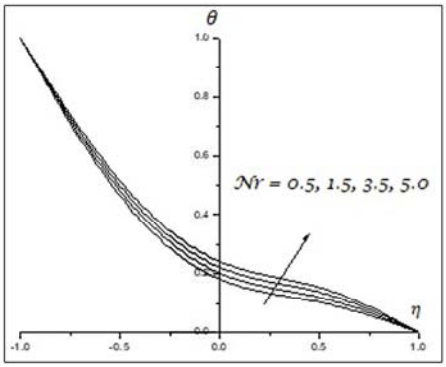

(c) Illustration of temperature (θ) versus N_r.

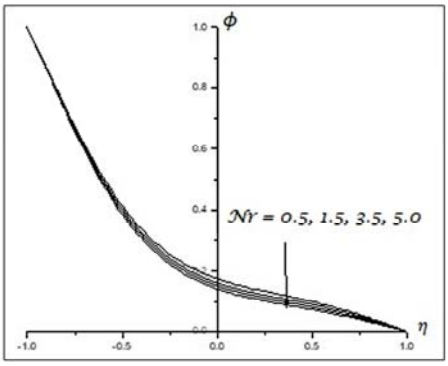

(d) Illustration of nano-particle concentration (φ) versus N_r.

Fig.2. $N = 1.0$, $A_{11} = 0.1$, $M = 0.5$, $B_{11} = 0.1$, $E_c = 0.01$, $R = 0.5$, $N_b = 0.1$, $Nt = 0.1$.

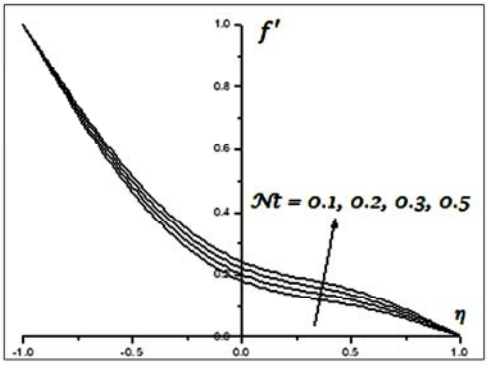

(a) Illustration of primary velocity (f') versus N_t.

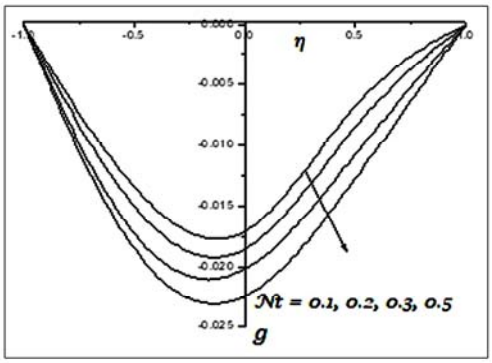

(b) Illustration of secondary velocity (g) versus N_t.

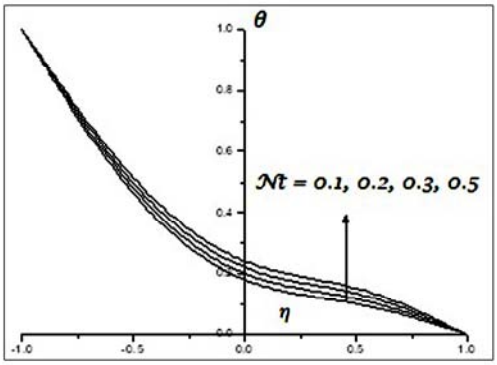

(c) Illustration of temperature (θ) versus N_t.

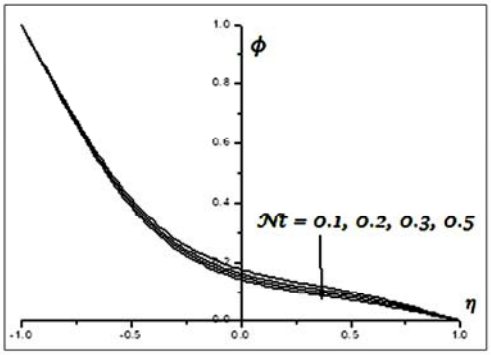

(d) Illustration of nano-particle concentration (φ) versus N_t.

Fig.3. $N_r = 0.5$, $N = 1.0$, $A_{11} = 0.1$, $M = 0.5$, $B_{11} = 0.1$, $E_c = 0.01$, $R = 0.5$, $N_b = 0.1$.

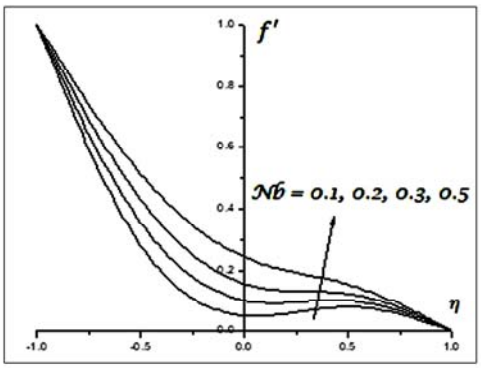

(a) Illustration of primary velocity (f') versus N_b.

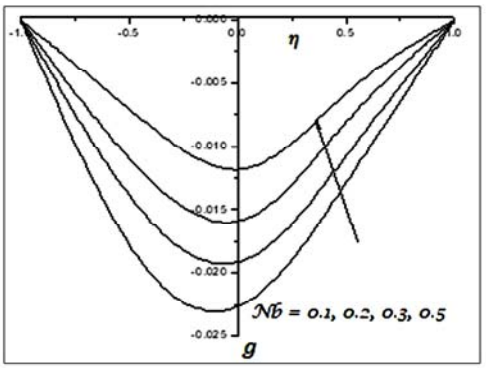

(b) Illustration of secondary velocity (g) versus N_b.

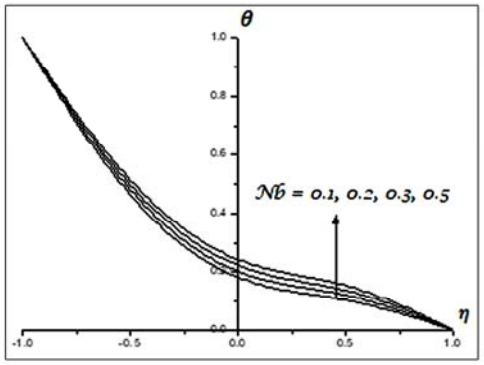

(c) Illustration of temperature (θ) versus N_b.

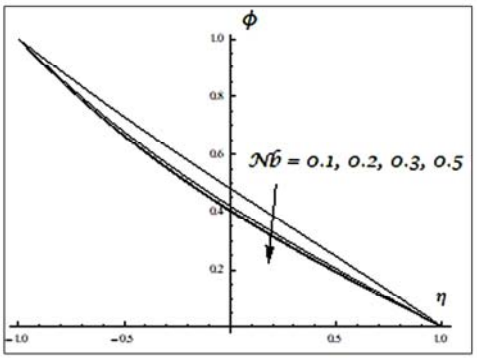

(d) Illustration of nano-particle concentration (φ) versus N_b

Fig.4. N_r= *0.5*, N = *1.0*, M = *0.5*, A_{11} = *0.1*, B_{11} = *0.1*, E_c = *0.01*, R = *0.5*, N_t = *0.1*.

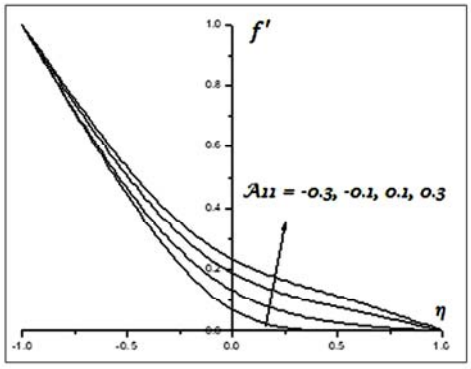

(a) Illustration of primary velocity (f') versus A_{11}.

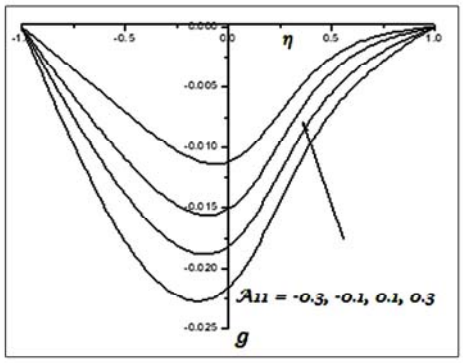

(b) Illustration of secondary velocity (g) versus A_{11}.

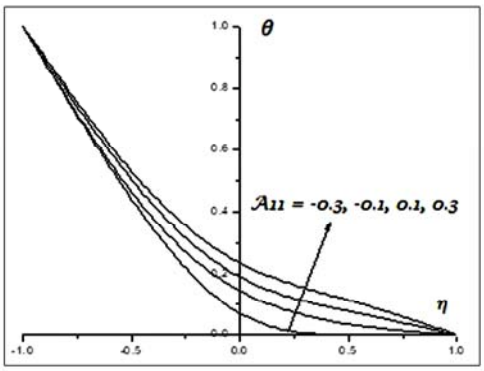

(c) Illustration of temperature (θ) versus A_{11}.

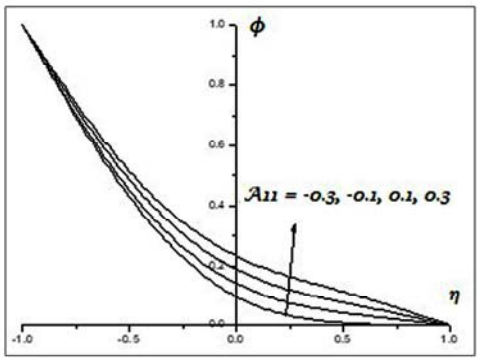

(d) Illustration of nano-particle concentration (φ) versus A_{11}.

Fig.5. N_r= *0.5*, N = *1.0*, M = *0.5*, G= *2.0*, f_w=*0.2*, B_{11} = *0.1*, E_c = *0.01*, R = *0.5*, N_b = *0.1*, N_t = *0.1*.

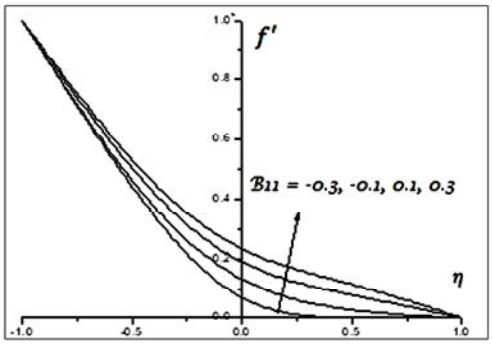

(a) Illustration of primary velocity (f') versus B_{11}.

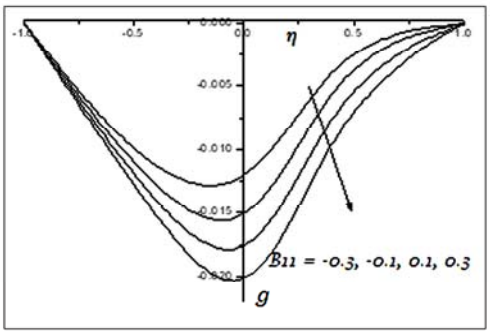

(b) Illustration of secondary velocity (g) versus B_{11}.

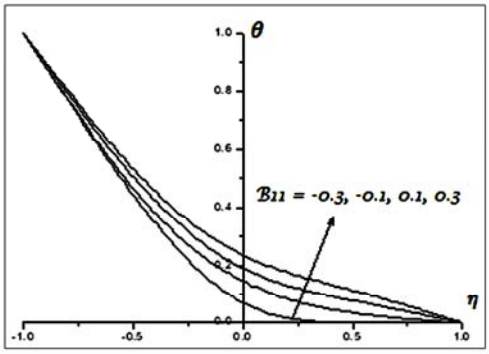

(c) Illustration of temperature (θ) versus B_{11}.

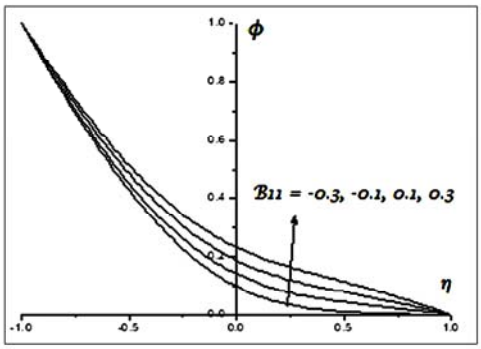

(d) Illustration of nano-particle concentration (φ) versus B_{11}.

Fig.6. N_r= *0.5*, N = *1.0*, M = *0.5*, G= *2.0*, A_{11} = *0.1*, E_c = *0.01*, R = *0.5*, N_b=*0.1*, N_t = *0.*

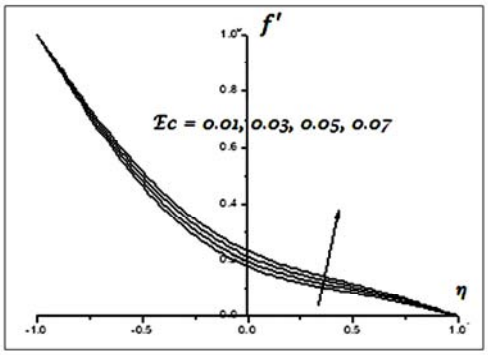

(a) Illustration of primary velocity (f') versus E_c.

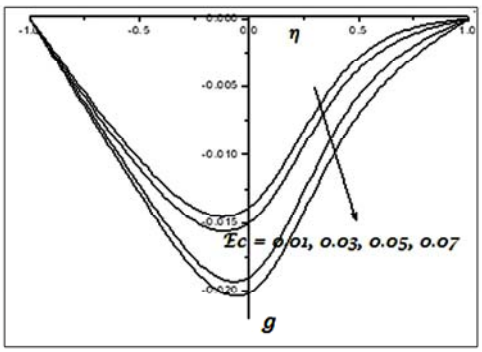

(b) Illustration of secondary velocity (g) versus E_c.

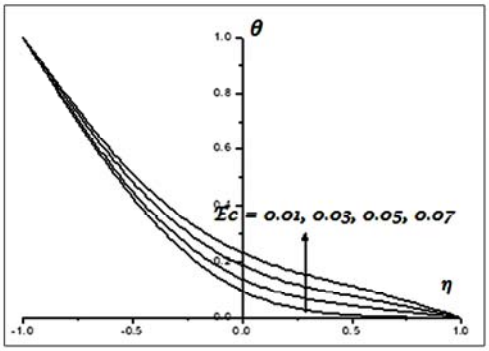

(c) Illustration of temperature (θ) versus E_c.

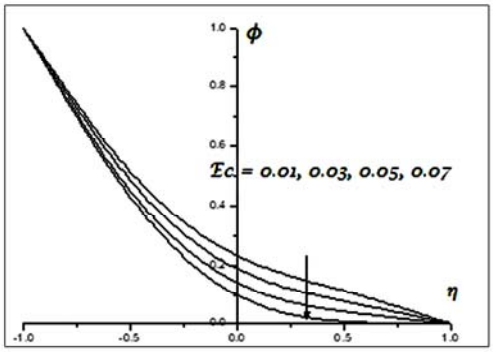

(d) Illustration of nano-particle concentration (φ) versus E_c.

Fig.7. N_r= 0.5, N = 1.0, M = 0.5, G= 2.0, A_{11} = 0.1, B_{11} = 0.1, R = 0.5, N_b=0.1, N_t = 0.1.

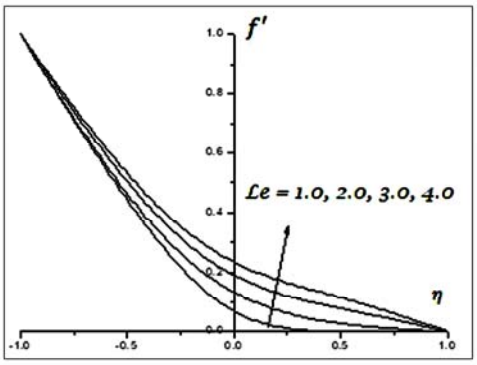

(a) Illustration of primary velocity (f') versus L_e.

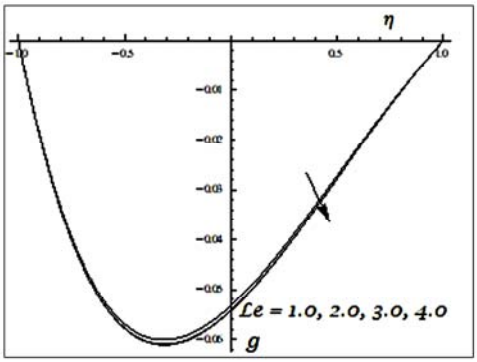

(b) Illustration of secondary velocity (g) versus L_e.

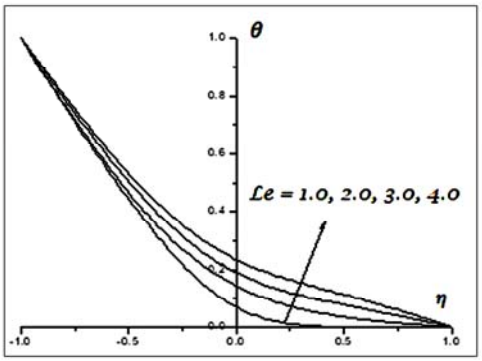

(c) Illustration of temperature (θ) versus L_e.

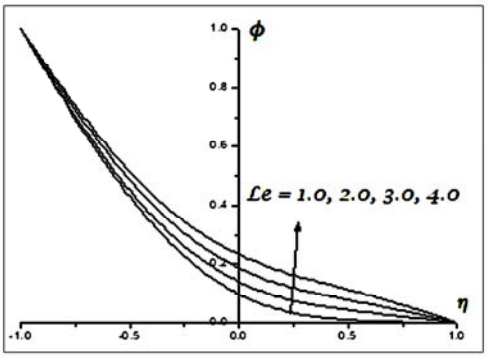

(d) Illustration of nano-particle concentration (φ) versus L_e.

Fig.8. N_r= 0.5, N = 1.0, M = 0.5, G= 2.0, A_{11} = 0.1, B_{11} = 0.1, R = 0.5, N_b=0.1, N_t = 0.1.

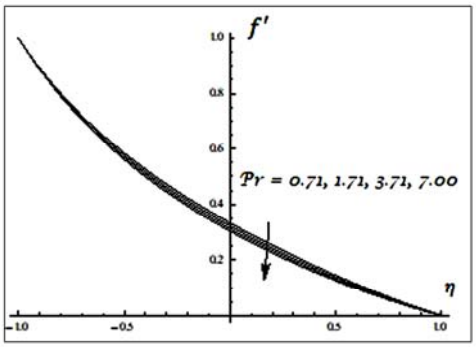

(a) Illustration of primary velocity (f') versus P_r.

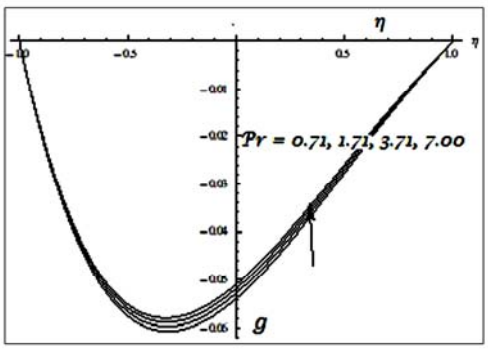

(b) Illustration of secondary velocity (g) versus P_r.

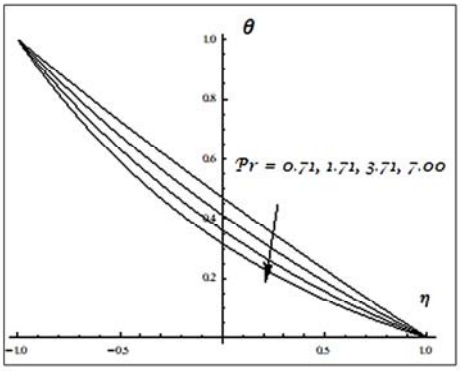

(c) Illustration of temperature (θ) versus Pr.

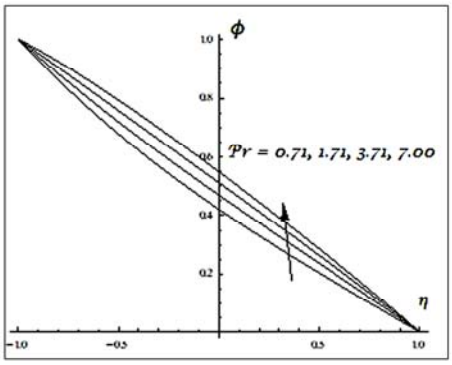

(d) Illustration of nan0-particle concentration (φ) versus P_r.

Fig.9. N_r= *0.5*, N = *1.0*, M = *0.5*, G= *2.0*, A_{11} = *0.1*, B_{11} = *0.1*, R = *0.5*, N_b=*0.1*, N_t = *0.1*.

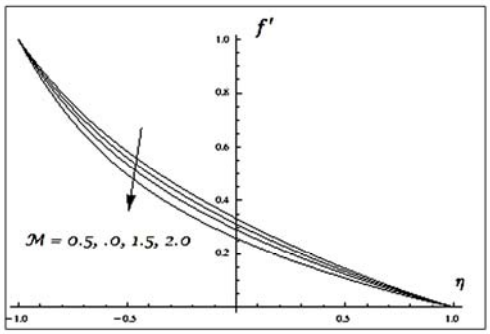

(a) Illustration of primary velocity (f') versus M.

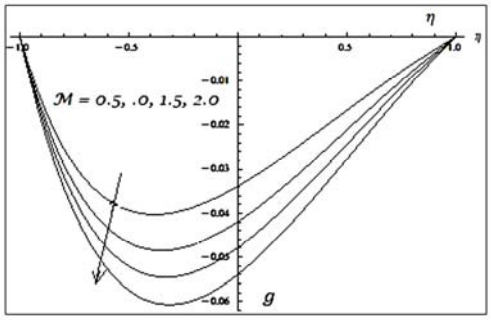

(b) Illustration of secondary velocity (g) versus M.

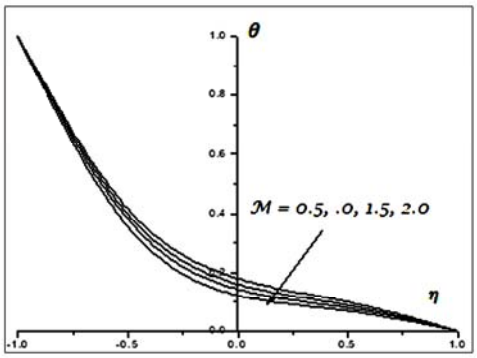

(c) Illustration of temperature (θ) versus M.

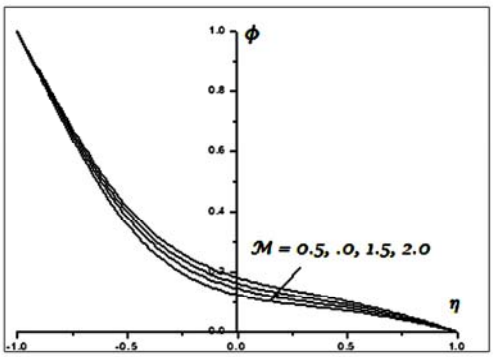

(d) Illustration of nano-particle concentration (φ) versus M.

Fig.10. N_r= *0.5*, N = *1.0*, G= *2.0*, A_{11} = *0.1*, B_{11} = *0.1*, R = *0.5*, E_c = *0.01*, N_b=*0.1*, N_t = *0.1*.

The skin frictions (τ_x, τ_z), heat transfer rate (Nusselt number (N_u)) and mass transfer rate (Sherwood number (S_h)) are presented (Tabs 1 and 2). It is observed that the skin friction components (τ_x, τ_z) and Nusselt number (N_u) decreases, but the Sherwood numeral (S_h) increases with a growth in the Brownian movement constraint (N_b) at η= *-1* and reverse outcomes are noted at η=*1*. This is due to the enhancement in velocities, temperature and a reduction in the nano-particle concentration profile. Moreover, the thermophoresis constraint (N_t) reduces the values of τ_z , N_u, and S_h, whereas improvements are noted in τ_x at η= *-1* but reverse results are seen at η=*1*.

From the table, it is noticed that an increment in Eckert number (E_c), emission constraint (N_r) increases τ_x and S_h but decreases τ_z and N_u. Furthermore, with a growth in the Prandtl number (P_r), τ_x and S_h decreases but τ_z and N_u increases. It is also noticed that τ_x and N_u drop, but τ_z and S_h enhance with an increase in the magnetic constraint (*M*). These constraints are computed at η= *-1* (Tab.1), whereas contrary results are seen in Tab.2 at η=*1*. These effects are in agreement with the results of [10] and [24].

Table 1. Heat transfer rate (Nusselt numeral (N_u)), skin friction, ($\tau_{x,\ z}$), and mass transfer rate (Sherwood numeral (S_h)) at η=*–1*.

Constraints		τ_x	τ_z	N_u	S_h
N_r	*0.5*	*-1.16001*	*-0.22003*	*0.573119*	*0.73137*
	1.5	*-1.15768*	*-0.220275*	*0.554481*	*0.747941*
	3.5	*-1.15582*	*-0.22047*	*0.539719*	*0.76106*
	5.0	*-1.14866*	*-0.238703*	*0.527162*	*0.772191*
N_b	*0.1*	*-1.15971*	*-0.220062*	*0.586746*	*0.566106*
	0.2	*-1.16001*	*-0.220083*	*0.573119*	*0.73137*
	0.3	*-1.17854*	*-0.220189*	*0.559834*	*0.764232*
	0.5	*-1.19167*	*-0.238466*	*0.545866*	*0.77855*
N_t	*0.1*	*-1.16354*	*-0.219646*	*0.598622*	*0.709005*
	0.2	*-1.15971*	*-0.220062*	*0.586746*	*0.566106*
	0.3	*-1.15651*	*-0.220407*	*0.57504*	*0.463665*
	0.5	*-1.1425*	*-0.238318*	*0.562333*	*0.407595*
E_c	*0.01*	*-1.16001*	*-0.22003*	*0.573119*	*0.73137*
	0.03	*-1.15985*	*-0.220046*	*0.571438*	*0.732913*
	0.05	*-1.1597*	*-0.220061*	*0.569758*	*0.734455*
	0.07	*-1.4428*	*-0.238105*	*0.566975*	*0.736955*
A_{11}	*0.1*	*-1.16001*	*-0.22003*	*0.573119*	*0.73137*
	0.3	*-1.15942*	*-0.22009*	*0.567993*	*0.735977*
	-0.1	*-1.1606*	*-0.219971*	*0.578242*	*0.726767*
	-0.3	*-1.19606*	*-0.217925*	*0.582244*	*0.723113*
B_{11}	*0.1*	*-1.16354*	*-0.219646*	*0.598622*	*0.709005*
	0.3	*-1.16279*	*-0.219724*	*0.592428*	*0.714531*
	-0.1	*-1.1643*	*-0.219569*	*0.604786*	*0.703504*
	-0.3	*-1.20033*	*-0.217457*	*0.610214*	*0.698617*
L_e	*1.0*	*-1.16354*	*-0.219646*	*0.598622*	*0.709005*
	2.0	*-1.1639*	*-0.219724*	*0.59992*	*0.70531*
	3.0	*-1.16434*	*-0.21999*	*0.604786*	*0.70504*
	4.0	*-1.20033*	*-0.22457*	*0.610214*	*0.698617*
P_r	*0.71*	*-1.16001*	*-0.22003*	*0.573119*	*0.73137*
	1.71	*-1.17947*	*-0.21794*	*0.722155*	*0.599516*
	3.71	*-1.1972*	*-0.216062*	*0.865775*	*0.471376*
	7.00	*-1.25243*	*-0.211881*	*0.999349*	*0.351101*
M	*0.5*	*-1.16201*	*-0.22123*	*0.573129*	*0.73237*
	1.0	*-1.2653*	*-0.205156*	*0.570211*	*0.744761*
	1.5	*-1.76374*	*-0.152015*	*0.557491*	*0.471376*
	2.0	*-1.99979*	*-0.135145*	*0.551985*	*0.749447*

Table 2. Heat transfer rate (Nusselt numeral (N_u)), skin friction, ($\tau_{x,\ z}$), and mass transfer rate Sherwood numeral (S_h)) at η=*1*.

Constraints		τ_x	τ_z	N_u	S_h
N_r	*0.5*	*-0.239542*	*0.047573*	*0.447817*	*0.409673*
	1.5	*-0.240991*	*0.047695*	*0.458234*	*0.40107*
	3.5	*-0.242144*	*0.0477918*	*0.46657*	*0.394178*
	5	*-0.23615*	*0.0472169*	*0.4740*	*0.388014*
N_b	*0.1*	*-0.239753*	*0.0475896*	*0.438682*	*0.521245*
	0.2	*-0.239542*	*0.047573*	*0.447817*	*0.409673*
	0.3	*-0.240522*	*0.0476542*	*0.456963*	*0.387345*
	0.5	*-0.234873*	*0.047104*	*0.46717*	*0.377383*
N_t	*0.1*	*-0.237115*	*0.047373*	*0.428597*	*0.425952*
	0.2	*-0.239753*	*0.0475896*	*0.438682*	*0.521245*
	0.3	*-0.241941*	*0.0477686*	*0.448989*	*0.581115*
	0.5	*-0.234104*	*0.0470354*	*0.460732*	*0.59707*
E_c	*0.01*	*-0.239542*	*0.047573*	*0.447817*	*0.409673*
	0.03	*-0.239626*	*0.0475803*	*0.448373*	*0.409226*
	0.05	*-0.23971*	*0.0475875*	*0.448929*	*0.408779*
	0.07	*-0.232595*	*0.0469144*	*0.450419*	*0.407541*
A_{11}	*0.1*	*-0.239542*	*0.047573*	*0.447817*	*0.409673*
	0.3	*-0.239869*	*0.0476014*	*0.449864*	*0.40805*
	-0.1	*-0.239216*	*0.0475447*	*0.445773*	*0.411294*
	-0.3	*-0.231625*	*0.0468287*	*0.444793*	*0.412015*
B_{11}	*0.1*	*-0.237115*	*0.047373*	*0.428597*	*0.425952*
	0.3	*-0.237551*	*0.0474107*	*0.431336*	*0.42377*
	-0.1	*-0.236683*	*0.0473355*	*0.425881*	*0.428115*
	-0.3	*-0.228696*	*0.0465826*	*0.423999*	*0.429566*
L_e	*1.0*	*-0.237115*	*0.047373*	*0.428597*	*0.425952*
	2.0	*-0.237551*	*0.0474107*	*0.431336*	*0.42377*
	3.0	*-0.236683*	*0.0473355*	*0.425881*	*0.428115*
	4.0	*-0.228696*	*0.0465826*	*0.423999*	*0.429566*
P_r	*0.71*	*-0.239542*	*0.047573*	*0.447817*	*0.409673*
	1.71	*-0.226719*	*0.046498*	*0.350203*	*0.491672*
	3.71	*-0.215748*	*0.0455451*	*0.273769*	*0.554697*
	7.00	*-0.196287*	*0.0437184*	*0.216996*	*0.60053*
M	*0.5*	*-0.237115*	*0.047337*	*0.448597*	*0. 409677*
	1.0	*-0.222416*	*0.0416007*	*0.450465*	*0.407431*
	1.5	*-0.152835*	*0.0214176*	*0.46183*	*0.397803*
	2.0	*-0.124507*	*0.0156673*	*0.466687*	*0.393686*

4. Conclusion

The conclusions are as follows:

- temperature, primary and secondary velocities rise and the concentration profile decreases with a growth in emission constraint, Brownian movement constraint and Eckert number,
- growth in thermophoresis constraint increases the primary velocity and temperature, whereas it reduces the secondary velocity and concentration profile,
- a similar behavior for primary and secondary velocity and dissimilar behavior of temperature and concentration profile on the Prandtl number,
- an opposite behavior of magnetic constraint is observed on velocity, temperature, and concentration profile,
- a similar effect on the primary velocity, concentration profile, and temperature, but dislike impact on secondary velocity are noticed for Lewis number, space, and temperature-dependent heat source constraint,

- the skin friction constraint descends with growth in magnetic constraint, Brownian movement constraint, Lewis number, Prandtl number,
- a dissimilar behavior of the heat transfer rate (N_u) noticed on emission constraint, Brownian movement constraint, Eckert number, space, and temperature-dependent heat source constraint, and magnetic constraint, but the parallel behavior on the Lewis number and Prandtl number,
- the mass transfer rate (S_h) rises with increase in Eckert number, emission and Brownian movement constraint, space, and temperature-dependent heat source constraint, while it decreases with an increase in thermophoresis constraint, Lewis number and Prandtl number.

Nomenclature

C – nano-particle concentration
C_1, C_2 – fixed concentration of conduit walls
D_b – themophoresis diffusion coefficient
G_r – Grashof number
g – gravity
H_0 – uniform magnetic strength
k – permeability of the medium
M – magnetic constraint
N – buoyancy ratio constraint
N_u – Nusselt number/heat transfer rate
R_m – magnetic Reynold's number
S_h – Sherwood number/mass transfer rate
T – temperature
T_1,T_2 – fixed temperature of left and right walls
T_m – average fluid temperature
u, v – velocities in x and y direction
β – thermal expansion coefficient
β^* – volume expansion coefficient
β_R – average absorption coefficient
μ – dynamic viscosity
μ_e – magnetic permeability
Υ – chemical response constraint
ρ & p – density and pressure
τ_x, τ_z – skin friction constraint
σ – electrical conductivity
σ^* – Stefan-Boltzman constant

References

[1] Choi S.U.S. (1995): *Enhancing thermal conductivity of fluids with nanoparticles with developments and applications of non-Newtonian flows.* – Proc. ASME Int. Mech. Engg. Congress Exposition, FED 231/MD, vol.49, pp.99-105.

[2] Eastman J.A., Choi S.U.S., Li S., Yu W. and Thompson L.J. (2001): *Anomalously increased effective thermal conductivity of ethylene glycol – based nanofluids containing copper nanoparticles.* – Appl. Phys. Lett. vol.78, No.6, pp.718-720.

[3] Keblinski P., Phillpot S.R., Choi S.U.S. and Eastman J.A. (2002): *Mechanisms of heat flow in suspensions of nano-sized particles (nano-fluids)*. – Int. J. Heat Mass Transf. vol. 45, No.4, pp.855-863.

[4] Buongiorno J. (2006): *Convective transport in nanofluids*. – J. Heat Transf. vol.128, pp.240-250.

[5] Kleinstreue C., Li J. and Koo J. (2008): *Microfluidics of nano-drug delivery.* – Int. J. Heat Mass Transf. vol.51, No.23, pp.5590-5597.

[6] Bachok N., Ishak A. and Pop I. (2010): *Boundary-layer flow of nanofluids over a moving surface in a flowing fluid*. – Int. J. Thermal Sci. vol.49, No.4, pp.1663-1668.

[7] Circar, Mukharjee (2008): *Effects of mass transfer and rotation on flow past a porous plate in a porous medium with variable suction in slip flow*. – Acta Cienc. Indica Math., vol.34, No.2, pp.737-751.

[8] Khan W.A. and Pop I. (2010): *Boundary-layer flow of a nanofluid past a stretching sheet*. – Int. J. Heat Mass Transf. vol.53, pp.2477-2483.

[9] Hamad M.A. and Ferdows M. (2011): *Similarity solution of boundary layer stagnation – point flow towards a heated porous stretching sheet saturated with a nanofluid with heat absorption/generation and suction/blowing: a lie group analysis*. – Comm. Nonlinear Sci. and Numer. Simu. vol.17, No.1, pp. 132-140.

[10] Makinde O.D. and Aziz A. (2011): *Boundary layer flow of a nanofluid past a stretching sheet with convective boundary condition*. – Int. J. Heat Mass Transf. vol.50, pp.1326-1332.

[11] Gorla R.S. and Chamkha A. (2011): *Natural convective boundary layer flow over a horizontal plate embedded in a porous medium saturated with a nanofluid*. – J. Modern Phys. vol.2, pp.62-71.

[12] MadhusudhanReddy Y. and PrasadRao D.R.V. (2012): *Effect of thermo diffusion and chemical reaction on non-Darcy convective heat and mass transfer flow in a vertical channel with radiation.* – Int. J. Math. Arch., vol.4, pp.1-13.

[13] Rana P. and Bhargava R. (2012): *Flow and heat transfer of a nanofluid over a nonlinearly stretching sheet: A numerical study*. – Comm. Nonlinear Sci. and Numer. Simu., vol.17, No.1, pp.212-226.

[14] Nadeem S. and Lee C. (2012): *Boundary layer flow of a nanofluid over an exponentially stretching surface*. – Nanoscale Res. Lett. vol.7, pp.1663-1668.

[15] Sankad G. and Dhange M. (2016): *Peristaltic pumping of an incompressible viscous fluid in a porous medium with wall effects and chemical reactions.* – Alexandria Eng. J. vol.55, pp.2015-2021.

[16] MadhaviLatha S. and Prasad Rao D.R.V. (2017): *Effect of chemical reaction and thermo-diffusion on convective heat and mass transfer flow of a rotating fluid through a porous medium in a vertical channel with stretching walls*. – Int. J. Math. Arch. vol.8, No.5, pp. 65-79.

[17] Sulochana C. and Ramnakrishna G.N. (2017): *Effect of heat sources on non-Darcy convective heat and mass transfer flow of Cuo-water and Al2O3-water nanofluids in vertical channel*. – Int. J. Emer. Trend. Eng. Dev. vol.63, No.7, pp.52-69.

[18] Hazem A.A. (1998): *Unsteady MHD flow near a rotating porous disk with uniform suction or injection*. – Fluid Dynam. Res., vol.23, No.5, pp.283-290.

[19] Mohan M. (1977): *Combined effects of free and forced convection on magneto hydrodynamic flow in a rotating channel*. – Proc. Indian Acad. Sci. vol.85, No.4, pp.383-401.

[20] PrasadRao D.R.V., Krishna D.V. and Debnath L. (1982): *Combined effect of free and forced convection on MHD flow in a rotating porous channel.* – Int. J. Math. Sci. vol.5, No.1, pp.165-182.

[21] Zanchini E. (1998): *Effect of viscous dissipation on mixed convection in a vertical channel with boundary conditions of the third kind*. – Int. J. Heat Mass Transf. vol.41, pp.3949-3959.

[22] Singh K.D. and Mathew (2009): *An oscillatory free convective MHD flow in a rotating vertical porous channel with heat source.* – Ganita. vol.60, No.1, pp.91-110.

[23] Kuznetsov A.V. and Nield D.A. (2010): *Natural convective boundary-layer flow of a nanofluid past a vertical plate*. – Int. J. Thermal Sci. vol.49, pp.243-247.

[24] Sreenivas Rao (2017): *MHD mixed convective heat and mass transfer in a vertical channel with stretching walls.* – Int. J. Res. Dev. Tech. vol.7, No.4, pp.21-32.

[25] Hamad M.A., Pop I. and Ismail A.I. (2011): *Magnetic field effects on convection flow of a nanofluid past a vertical semi-infinite flat plate.* – Nonlinear Anal. Real World Appl., vol.12, pp.1338-1346.

Received: April 13, 2020

Revised: July 29, 2020